Static and dynamical susceptibility of $LaO_{1-x}F_xFeAs$

M. Monni,[1] F. Bernardini,[1] G. Profeta,[2] A. Sanna,[1,3,4,5] S. Sharma,[3,5] J. K. Dewhurst,[3,4,5] C. Bersier,[3,4,5] A. Continenza,[2] E. K. U. Gross,[3,5] and S. Massidda[1]

[1]*CNR-IOM SLACS, and Dipartimento di Fisica, Università degli Studi di Cagliari, I-09042 Monserrato (CA), Italy*

[2]*CNISM, Dipartimento di Fisica, Università degli Studi dell'Aquila, Via Vetoio 10, Coppito, I-67010 L'Aquila, Italy*

[3]*Institut für Theoretische Physik, Freie Universität Berlin, Arnimallee 14, D-14195 Berlin, Germany*

[4]*Fritz Haber Institute of the Max Planck Society, Faradayweg 4-6, D-14195 Berlin, Germany*

[5]*Max-Planck-Institut für Mikrostrukturphysik, Weinberg 2, D-06120 Halle, Germany*

(Received 7 January 2010; revised manuscript received 8 February 2010; published 4 March 2010)

The mechanism of superconductivity and magnetism and their possible interplay have recently been under debate in pnictides. A likely pairing mechanism includes an important role of spin fluctuations and can be expressed in terms of the magnetic susceptibility χ. The latter is therefore a key quantity in the determination of both the magnetic properties of the system in the normal state and of the contribution of spin fluctuations to the pairing potential. A basic ingredient to obtain χ is the independent-electron susceptibility χ_0. Using $LaO_{1-x}F_xFeAs$ as a prototype material, in this report we present a detailed *ab initio* study of $\chi_0(\mathbf{q},\omega)$ as a function of doping and of the internal atomic positions. The resulting static $\chi_0(\mathbf{q},0)$ is consistent with both the observed M-point-related magnetic stripe phase in the parent compound and with the existence of incommensurate magnetic structures predicted by *ab initio* calculations upon doping.

DOI: 10.1103/PhysRevB.81.104503 PACS number(s): 74.20.Pq, 74.70.Xa, 75.40.Cx, 75.40.Gb

I. INTRODUCTION

Iron pnictides[1] represent a challenge in the field of superconductivity, both from the experimental and theoretical point of view.[2,3] They are magnetic metals that upon electron (e) or hole (h) doping transform into high-temperature superconductors. The prototype of this new family of superconductors is LaOFeAs,[1] which superconducts at 26 K upon partial substitution ($\approx$14%) of O with F. Several other superconducting pnictides have since been discovered, with a record critical temperature up to $T_c \approx 55$ K.[4] The parent undoped compound for these superconductors are antiferromagnetic (AFM) semimetals, with several competing magnetic structures lying within a few tens of a millielectron volt.[5–12] This is an ideal situation for the presence of magnetic instabilities with a strong possibility of spin fluctuations playing an important role. In fact this is confirmed by experiments, which show that the suppression of the magnetic instability is a necessary step to obtain superconductivity.[13,14]

This proximity to an AFM instability leads one to draw parallels between pnictides and cuprates. Despite several similarities these two families of superconductors show important differences. One of the most important differences is related to electronic correlations; cuprates are well known to be strongly correlated materials, where a treatment of on site Coulomb interactions is essential to get the correct normal ground state. On the other hand in the case of pnictides it was concluded by Anisimov *et al.*[15] that the electronic structure of these materials is consistent with a small value of the Coulomb interaction U (within the local density approximation combined with dynamical mean-field theory scheme LDA+DMFT) indicating that strong correlations may not be essential to describe them. In fact, unlike in cuprates, standard local/semilocal functionals within density-functional theory (DFT) can describe the occurrence of magnetism in pnictides, although the agreement between the calculated and the experimental magnetic moment and its dependence on the choice of functional and atomic positions has been extensively discussed.[2,6]

There is not a general consensus about the mechanism leading to superconductivity in these materials. It seems clear, however, that the electron-phonon interaction alone (without involvement of spins) is too weak[16] to produce such a high T_c, at least within the standard Migdal-Eliashberg theory. On the other hand explicit involvement of the spin degree of freedom leads to an enhancement of electron-phonon coupling;[17,18] therefore the role of phonons has not been completely ruled out.

However, the presence of a weak electron-phonon coupling at least in the classic sense lead to the suggestion of several alternative mechanisms which are essentially electronic in nature. Among these alternatives one of the most prominent is the mechanism suggested by Mazin *et al.*;[8] inspired by the peculiar shape of the Fermi surface (FS) (Ref. 19) they suggested an $s_\pm$ superconducting order parameter, having different sign on the h- and e-like sheets forming the FS. In this way superconductivity can be driven by a strong repulsive interband interaction (like spin fluctuations). The role of spin fluctuations in the Cooper pairing was proposed several years ago by Berk and Schrieffer;[20] this mechanism requires a nonconventional (i.e., not a simple s-wave) superconducting order parameter. The effective Hamiltonian of a system close to a magnetic instability "pairs" states at $\mathbf{k}$ and $\mathbf{k}+\mathbf{q}$ by an effective interaction matrix element, ultimately related to the $\mathbf{q}$ vector and frequency-dependent susceptibility $\chi(\mathbf{q},\omega)$. Both the $\mathbf{q}$ vector and frequency dependence of χ are important in determining the symmetry and possibly the anisotropy of the superconducting gap on the FS. Experiments, on the other hand, cannot make a definite statement on the symmetry of the order parameter[2,3] making it difficult to validate/invalidate this scenario.

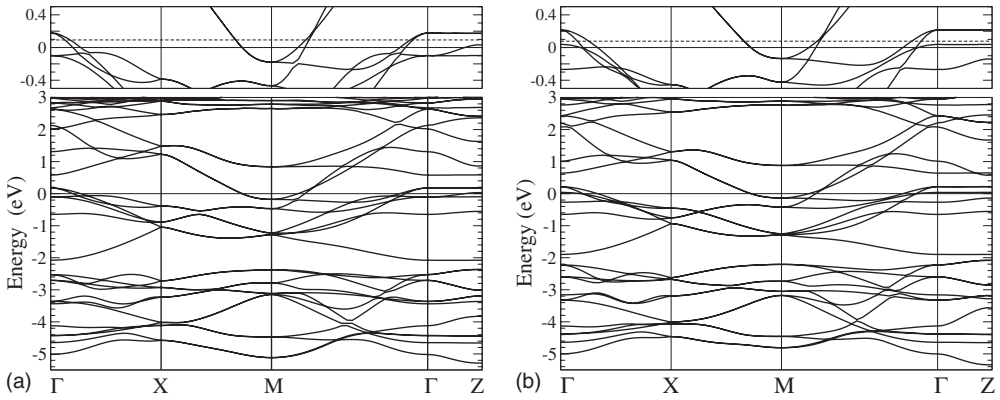

FIG. 1. Energy bands of LaOFeAs, for the theoretically optimized (left) and experimental position (right) of the As atom, along various symmetry directions in the Brillouin zone. The upper panel highlights the region around the Fermi level. Dashed line in the upper panel indicates the position of the Fermi level for the 14% doped LaOFeAs.

It is clear that the above-mentioned electronic mechanisms rely crucially on the detailed knowledge of the susceptibility, $\chi(\mathbf{q},\omega)$. Several calculations of the static χ have been reported on pnictides. The first *ab initio* calculation of the $\chi(\mathbf{q},0)$ did not include matrix elements among Bloch states.[8] Later calculations of the static χ_0 were based on either approximate calculation of matrix elements[11] or on tight-binding fits of the minimal bands manifold around E_F,[21–23] without inclusion of higher energy interband transitions. This latter approach suffers from the fact that, even though the main structure of the static $\chi(\mathbf{q},0)$ can be determined by low-energy transitions (without including many empty bands) no definite conclusions can be reached about the structure of $\chi(\mathbf{q},\omega)$. Hence, an *ab initio* investigation of the full dynamical susceptibility, including a proper account of the matrix elements involving Bloch states is highly desirable and is still lacking. To fill this gap, in this paper we present an *ab initio* determination of the static- and dynamical-independent-electron susceptibility of LaOFeAs, based on electronic-structure calculations performed within DFT. Our results are a step toward an understanding of the material properties and of the possible contribution of spin fluctuations to the superconducting pairing.

The rest of the paper is organized as follows: Sec. II discusses the methodology and computational details. Section III contains the results. In particular, first the static susceptibility $\chi_0(\mathbf{q},0)$ is discussed and then the results for the real and imaginary parts of χ_0 as a function of frequency are presented. Finally the conclusions are given in Sec. IV.

II. METHOD

The independent-electron susceptibility is defined as

$$\chi_0(\mathbf{q},\mathbf{G},\mathbf{G}',\omega) = \sum_{nn'\mathbf{k}} \frac{f_{n\mathbf{k}} - f_{n'\mathbf{k}+\mathbf{q}}}{\epsilon_{n\mathbf{k}} - \epsilon_{n'\mathbf{k}+\mathbf{q}} + \hbar(\omega + i\eta)} \times \langle n'\mathbf{k}+\mathbf{q}|e^{i(\mathbf{q}+\mathbf{G})\cdot\mathbf{r}}|n\mathbf{k}\rangle\langle n\mathbf{k}|e^{-i(\mathbf{q}+\mathbf{G}')\cdot\mathbf{r}}|n'\mathbf{k}+\mathbf{q}\rangle, \quad (1)$$

where $\epsilon_{n\mathbf{k}}$ and $f_{n\mathbf{k}}$ are the one-electron energies and the corresponding Fermi functions, and $\mathbf{G}$ and $\mathbf{G}'$ are reciprocal-lattice vectors. In this work we accurately compute χ_0 by performing the summations in Eq. (1) using a random sampling over the Brillouin zone (BZ). We used ~3000 independent $\mathbf{k}$ points per band, chosen according to a stochastic algorithm which accumulates them around the FS for bands crossing E_F. The final results are obtained by averaging over 40 runs each containing completely independent $\mathbf{k}$-point set. This procedure nearly completely eliminates the numerical noise and shows a good convergence both in terms of number of independent runs and number of $\mathbf{k}$ points within a single run. We have included 65 bands in order to ensure convergence with respect to the number of empty bands.

The energy bands and the matrix elements for LaOFeAs have been calculated, within the (spin-independent) local-density approximation[24] to the exchange-correlation functional. Our calculations have been done using the full-potential linearized augmented plane-wave method. This choice is necessary because of the extreme sensitivity of the electronic structure (in particular, of the bands close to E_F) to the method.[25] No numerical approximation has been made in the evaluation of matrix elements in Eq. (1). Given the huge debate about the dependence of the results on the position of the As atom in the unit cell,[25,26] in the present work we show results both for the theoretically optimized (z_{As}=0.638) and experimental[27] (z_{As}=0.6513) position of the As atom.

III. RESULTS AND DISCUSSION

We first look at the band structure and the FS for the parent and the doped LaOFeAs. The ground-state calculations are performed with the tetragonal unit cell, containing two Fe atoms, at the experimental lattice constants a =4.03 Å and c/a=2.166. The energy bands of LaOFeAs calculated using both z_{As} are shown in Fig. 1. Four bands cross the Fermi level E_F, having predominantly Fe d character moderately hybridized with As p. These band structures are in agreement with previous results.[16,25]

The corresponding FS are given in Fig. 2. The FS calculated with optimized and experimental z_{As} for the undoped compound are quite similar with two e-like cylinders around the M point and two h-like cylinders warped around the Γ point of the BZ. However, the two FS differ when it comes to

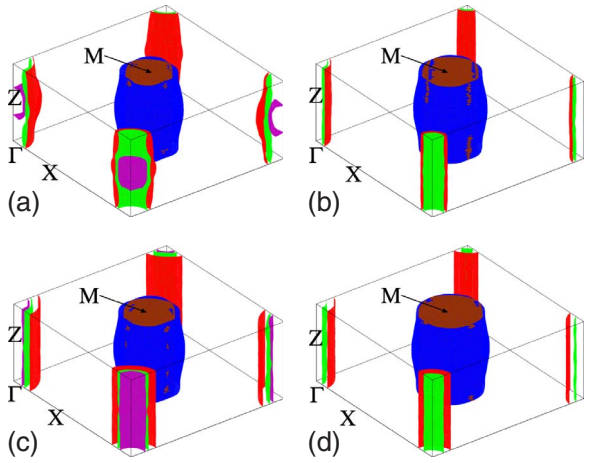

FIG. 2. (Color online) Fermi surface of $LaO_{1-x}F_xFeAs$. Top panel: at theoretically optimized position of the As atom with (a) $x=0$ and (b) $x=0.14$. Bottom panel: at experimental position of the As atom with (c) $x=0$ and (d) $x=0.14$.

the third h-like manifold which appears as a three-dimensional (3D) structure on the use of optimized As positions and as a two-dimensional (2D) cylinder when the experimental atomic positions are used.

Since the parent compound becomes superconducting on electron doping, it is important to look at the change in the electronic structure as a function of the fluorine content. The doping is treated by the means of rigid-band model which is a reasonable approximation for LaOFeAs.[28] As for the crystal structure, it is kept fixed to the undoped values even for the doped case. This choice is justified for the material under investigation; it was shown by Mazin *et al.*[25] that the lattice parameter and atomic positions are not sensitive to the doping. The FS for the 14% doped compound is shown in Fig. 2. Even though the undoped FS calculated using optimized and experimental z_{As} are substantially different, the doped FS for the two cases are fairly similar. The h-like FS sheet around Γ point for $x=0$ quickly disappears on electron doping in both cases (z_{As} optimized and experimental) with only 2D tubular structures around the Γ-Z (h-like) and the M-A (e-like) lines surviving. Most noticeably the nesting between h-like and e-like FS present in the undoped material becomes less prominent on doping due to the increase in the asymmetry between the e-like and the h-like cylinders.

A. Static response function

In order to elucidate how this change in FS upon doping manifests itself in the response of the material, in Figs. 3 and 4 are shown the response function $\chi_0(\mathbf{q},0)$ for $LaO_{1-x}F_xFeAs$ at $x=0$ and 0.14. Looking first at the undoped case, $x=0$ [Fig. 3(a)], two main features are clearly visible; first is the presence of a wide flat structure around the Γ and a relatively sharper peak around M point and second is the flatness of the response function in the c axis (tetragonal axis). As expected, due to the 2D nature of this material similar features (structures around Z and R points in otherwise flat response function) are also visible in the top plane [Fig. 3(b)]. These main features of the response function can be explained on the basis of the electronic structure of LaOFeAs and by comparison with the noninteracting electron gas.[29] The flat region near the zone center (Γ) is due to self-nesting of the FS cylinders. This scenario is similar to the 2D electron gas where the circular FS leads to a flat response with a sharp drop to zero at $2k_F$. In the present case, however, this drop is smooth due to different sizes and irregularities in shape of the FS cylinders. The broad peak in the χ at M point is due to the strong nesting between holelike and electronlike FS sheets. The presence of a perfect nesting, which is not realized in this material,[6,11] would give a diverging response at this point.

Doping [see Fig. 4(a)] leads to asymmetric change in the size of the electron and the hole FS cylinders which manifests itself as a craterlike structure around Γ point which continuously increases on going toward M/X points in the BZ. This monotonous increase in χ_0 with $|q|$ indicates the predominance of interband transitions. As this interband nesting becomes less perfect upon doping (worse matching of e and h FS), it produces a volcanolike feature around the M point. This feature, of the maximum being shifted away from the M point, is indicative of a possibility of an incommensurate spin configuration in this material. Interestingly, this incommensuration has been recently predicted from two different *ab initio* calculations.[6,11] The flatness of $\chi_0(\mathbf{q},0)$ in the remaining $\mathbf{q}$ space is consistent with the fact that all the competing magnetic structures lie within a small energy range, with in-plane $\mathbf{q}$ vector.

In order to understand the evolution of the features around the Γ and M points as a function of doping it is instructive to consider the contribution from different energy-wave-vector regions to χ_0. To study this we separate the contributions of

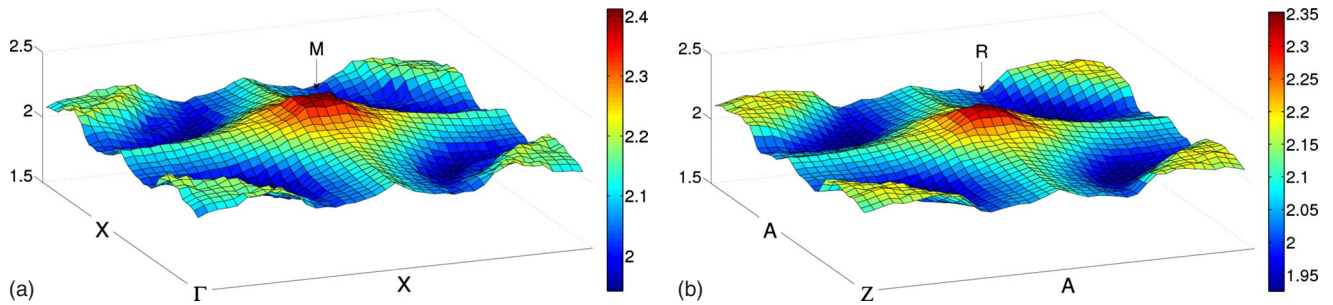

FIG. 3. (Color online) Real part of $\chi(\mathbf{q},0)$ for undoped LaOFeAs (a) on the basal plane (i.e., $q_z=0$) and (b) on the top plane (i.e., $q_z=\frac{\pi}{c}$).

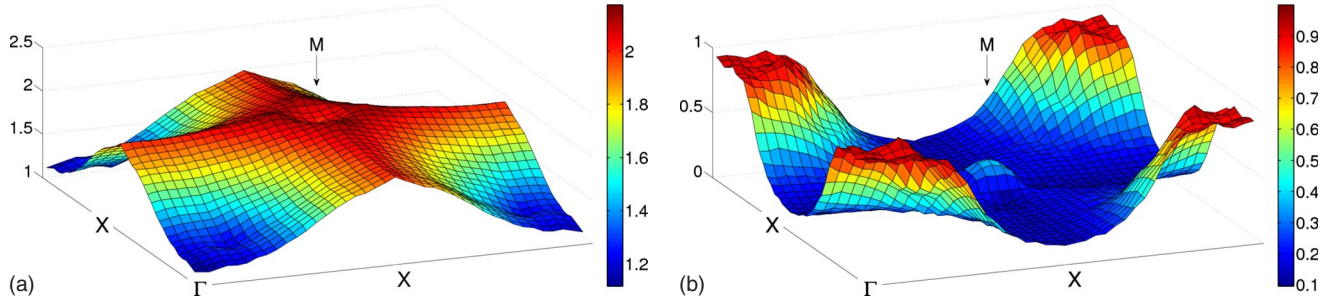

FIG. 4. (Color online) (a) Real part of $\chi(\mathbf{q},0)$ for 14% doped LaOFeAs and (b) $\Delta\chi_0$: the difference between the real part of χ for the doped and undoped LaOFeAs. The results are plotted on the basal plane.

different intraband and interband electronic transitions by separating the bands as follows: the first set consists of the two bands forming *h*-like FS sheets plus all the occupied bands and the second set consists of the all bands forming electronlike FS plus all the empty bands. Clearly such a grouping of the bands disregards band crossings (e.g., those of the *e* bands with filled states around M). Figure 5 shows static susceptibility resolved according to this criterion. Looking at various contributions around the Γ point it becomes clear that in both doped and undoped cases the low-momentum susceptibility is dominated by the intraband contribution (*e*-*e* and *h*-*h*). Doping leads to a strong reduction in the *h*-*h* contribution, which is expected since the effect of doping is to shrink the hole FS sheets around the Γ point. On the other hand around the M point and in the rest of the plane the interband *e*-*h* contributions dominate. Upon doping this interband contribution does not change substantially except in the very vicinity of the M point where a volcanolike feature is formed. This can be easily understood as a consequence of the change in shape of the FS upon doping; the asymmetry between the *e* and *h* sheets becomes stronger resulting in a reduction in the strength of the nesting.

In order to investigate how the response of $LaO_{1-x}F_xFeAs$ is affected by the change in atomic positions, we also calculate the $\chi_0^{(exp)}$ at the experimental position of the As atom. In Fig. 6 we plot $\chi_0^{(exp)}$ (in the basal plane) as a function of doping and its change relative to the χ_0 calculated at the optimized position of the As atom. We see a sizeable difference between the two at zero doping: using experimental positions, the peak at the nesting vector is much more evident and broader while the peak around Γ is depressed. We can relate this change to the differences in the electronic structure, the 3D bands crossing E_F around the Z point become 2D but also the radius of the FS cylinders is larger in the optimized structure making the nesting between *e*-like and *h*-like sheets less efficient. In the doped system, on the other hand, this band is completely full in both atomic configurations as a consequence of which in the doped case, the difference induced by change in atomic positions is not as significant.

On comparing the static susceptibility calculated in the present work with the previous results of Mazin *et al.*[8] one notices that the height of the peak around the M point is significantly suppressed on inclusion of the matrix elements. This is a consequence of the fact that the states near E_F contribute to Re χ_0 selectively, weighted by their overlap integral and not by unity. We also find that on approximate inclusion of matrix elements[11] the general shape and the dop-

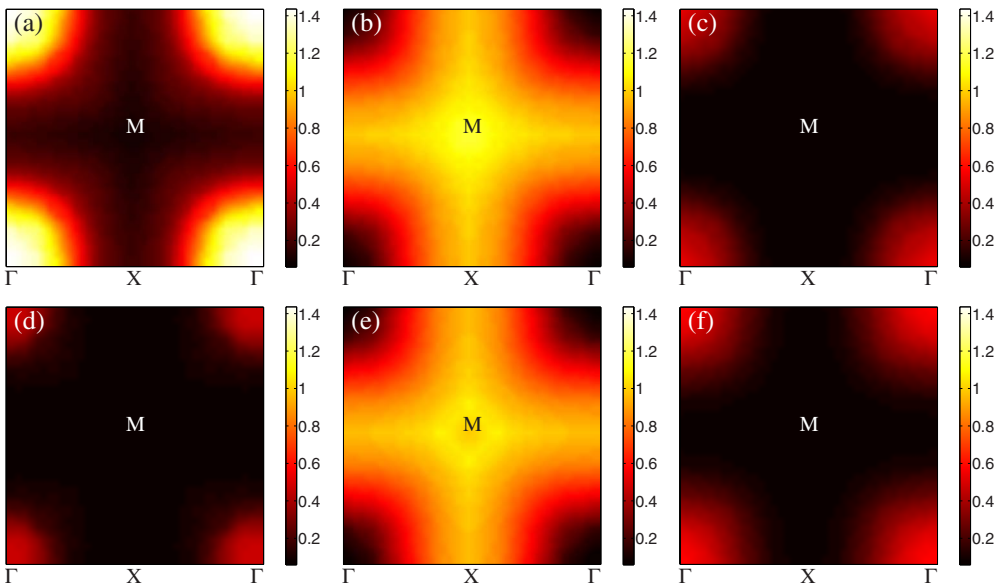

FIG. 5. (Color online) Intraband and interband contributions to $\chi_0(\mathbf{q},0)$, top panel for undoped and bottom panel for 14% doped LaOFeAs. (a) and (d) are *e*-*e*, (b) and (e) are *e*-*h*, and (c) and (f) are *h*-*h* contributions.

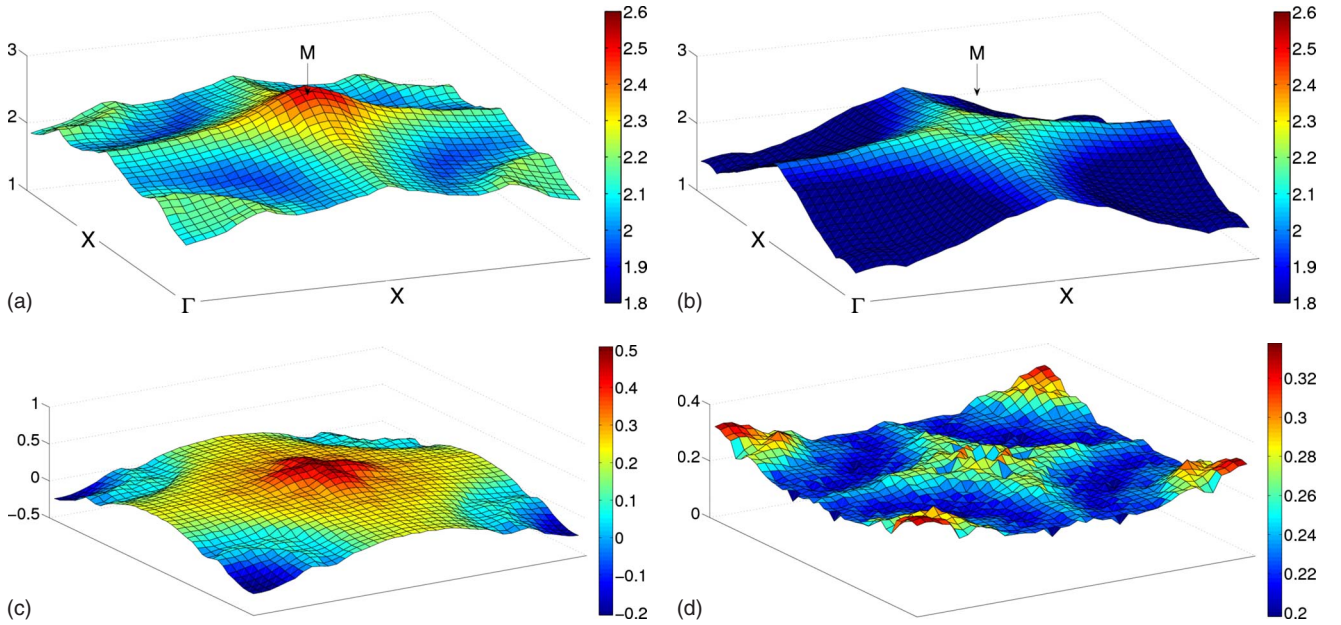

FIG. 6. (Color online) Real part of $\chi(\mathbf{q},0)$ on the basal plane (i.e., $q_z=0$), calculated using the experimental position of the As atom. Top panel: (a) for the undoped case and (b) for the 14% doped case. Bottom panel: (c) difference between (a) and same calculated at the theoretically optimized position of the As atom and (d) difference between (b) and same calculated at the theoretically optimized position of the As atom.

ing dependent evolution of the peak around M ($\overline{\mathrm{X}}$ in their convention for the BZ) is, after zone folding, in reasonable agreement with the present results.

It is believed that the interacting susceptibility is a key quantity in determining the effective electron-electron interactions leading to superconductivity. Our results show that the inclusion of the matrix elements influences its $\mathbf{q}$ dependence and, in particular, the relative height of the peaks. Although our calculations only refer to the independent-electron susceptibility, these conclusions are likely to hold also for the interacting χ. Therefore, it is important to include the matrix elements in order to use χ for assessing the validity of models for the superconducting mechanism (e.g., the $s_{\pm}$ wave).

B. Dynamical susceptibility

An overview of the dynamical response of the system is given in Fig. 7, where we plot Im χ_0, the imaginary part of $\chi_0(\mathbf{q},\omega)$, as a function of frequency and momentum, along the Γ-M-Γ and Γ-X-Γ lines of the Brillouin zone, for $x=0$. The most prominent structure is a broad peak located at frequencies between 1 and 2 eV, which behaves in a similar manner along the Γ-M-Γ and Γ-X-Γ directions. Near the M point we also see a sharp and intense peak located at about 3 eV. At this point it is also worth mentioning that the flat La $4f$ bands visible at around 3 eV in Fig. 1 do not result into any evident structure in the Im χ_0 plot, indicating the small hybridization (thereby small matrix element) of these states with Fe and As states.

At small values of $\mathbf{q}$ and at low frequency, the value of Im χ_0 grows linearly as a function of the frequency and then drops rapidly to zero (resembling linear-response susceptibility for the noninteracting electron gas). From Fig. 7(a), we see that this low-frequency feature has two components; the position of the first peak grows with $\mathbf{q}$, saturating at a frequency of ~0.4 eV while the second one grows up to ~1 eV finally merging into the main broad peak. This behavior is the same along the Γ-M-Γ and Γ-X-Γ lines, except for the presence of an extra low-frequency structure ($\omega \leq 0.3$ eV) visible around the M point. A detailed view of Im $\chi_0(\mathbf{q},\omega)$ and the behavior of Re $\chi_0(\mathbf{q},\omega)$ is given in Fig. 7(b) at X and M, both for the undoped and for the doped systems. Even though doping does not significantly change the general shape of both real and imaginary parts of χ_0, in

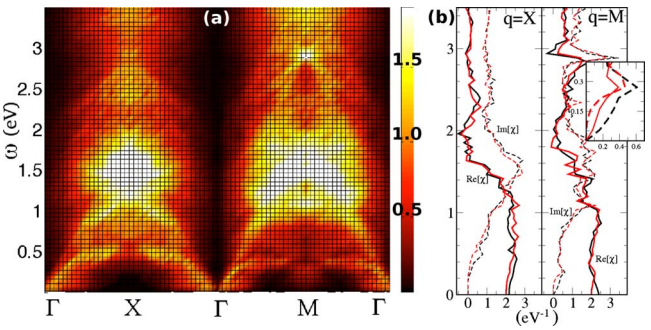

FIG. 7. (Color online) (a) Imaginary part of $\chi_0(\mathbf{q},\omega)$ (electron volt), for undoped LaOFeAs, as a function of $\mathbf{q}$ and ω. Results are plotted along Γ-X-Γ-M-Γ directions. (b) Plot of the real and imaginary parts of χ_0 as a function of ω for $\mathbf{q}$ corresponding to the X and M points of the BZ. Black and red refer to $x=0$ and 0.14, respectively. The inset of (b) shows the low-frequency part of χ_0 at M for $x=0$ and 0.14 [black and red (gray) dashed, respectively] and at one $\mathbf{q}$ point close to M corresponding to the edge of the volcano-like structure of Re χ_0 [thin red (gray) continuous line].

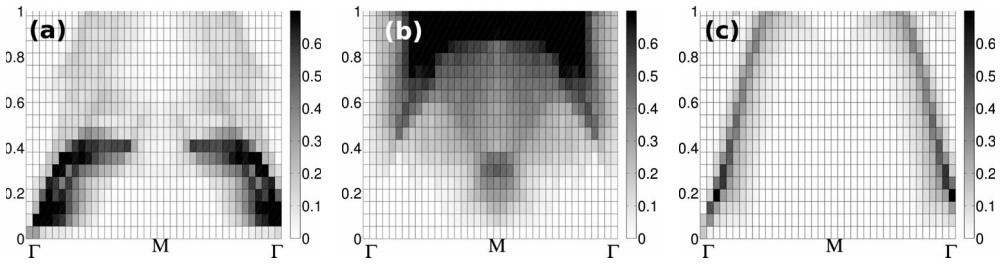

FIG. 8. Imaginary part of $\chi_0(\mathbf{q},\omega)$ (electron volt) decomposed into the intraband and interband contributions. Results are plotted along Γ-M-Γ direction. (a) *h-h*, (b) *e-h*, and (c) *e-e* contributions.

the low-frequency region, we notice a different behavior of Im $\chi_0(\mathbf{q},\omega)$ at M [see inset of Fig. 7(b)]. For $x=0$ the Im χ_0 grows linearly as a function of ω while it only starts to grow at a finite value of ω for $x=0.14$. The reason for this is closely tied to the nesting function; an highly nested FS gives rise to linear behavior for $x=0$. While in the doped case, deterioration of FS nesting at M, only allows finite-energy excitations, leading to a finite starting value for the Im $\chi_0(\mathbf{q},\omega)$. Interestingly, if we move slightly away from M (on the edges of the volcano structure discussed above), we recover a linear trend starting at $\omega=0$.

The band decomposition of Im $\chi_0(\mathbf{q},\omega)$, reported in Fig. 8 along the Γ-M-Γ line, shows that the interband (*e-h*) contributions dominate the high-frequency part and are also responsible for the low-frequency peak around M. The two dispersive peaks at low frequency discussed above originate from the intraband transitions (*e-e* and *h-h*); in particular, the relatively high-frequency branch comes mainly from electronic bands while the low-frequency one from hole bands. Figure 8 clearly shows that the *h-h* and *e-e* contributions are quite asymmetric; this asymmetry is clearly a consequence of the richness of the electronic structure of LaOFeAs near E_F.

IV. CONCLUSION

In summary, we report detailed calculations of the independent-electron susceptibility of nonmagnetic $LaO_{1-x}F_xFeAs$ as a function of doping and of the atomic positions within the unit cell. Our results are based on accurate electronic structure calculations within density-functional theory and include matrix elements from full-potential linearized augmented plane-wave method. We account properly for Fermi-surface-related features through an accurate sampling of the Brillouin zone.

The static susceptibility is peaked around the zone center and at the nesting vector $\mathbf{q}_N$ (M point) due to intraband (*e-e* and *h-h*) and interband transitions respectively, and is consistent with the observed stripe AFM ordering. However, the peak at M point is not as pronounced as reported in calculations with approximate or no matrix elements. Upon doping, the peak at M evolves into a volcanolike structure consistent with the incommensurate magnetic spiral state predicted by first-principle calculations. The intraband and interband analyses of the contributions to $\chi_0(q,0)$ shows an *e* versus *h* asymmetry which may relate to the multigap character suggested by experiments. Our results are a step toward the definition of an *ab initio* effective electron-electron interaction, necessary to obtain the pairing potential in pnictides.

ACKNOWLEDGMENTS

We acknowledge computational support by COSMOLAB consortium (Cagliari, Italy), by INFM-CNR through a supercomputing grant at Cineca (Bologna, Italy), by the Deutsche Forschungsgemeinschaft, and by NANOQUANTA Network of Excellence. F.B. acknowledges CASPUR for support by the HPC grant 2009. M.M. acknowledges support from the Regione Sardegna through the "Master and Back" program.

[1] Y. Kamihara, T. Watanabe, M. Hirano, and H. Hosono, J. Am. Chem. Soc. **130**, 3296 (2008).
[2] I. I. Mazin and J. Schmalian, Physica C **469**, 614 (2009).
[3] K. Ishida, Y. Nakai, and H. Osono, J. Phys. Soc. Jpn. **78**, 062001 (2009).
[4] Z.-A. Ren, W. Lu, J. Yang, W. Yi, X.-L. Shen, Z.-C. Li, G.-C. Che, X.-L. Dong, L.-L. Sun, F. Zhou, and Z.-X. Zhao, Chin. Phys. Lett. **25**, 2215 (2008); X. H. Chen, T. Wu, G. Wu, R. H. Liu, H. Chen, and D. F. Fang, Nature (London) **453**, 761 (2008); M. Rotter, M. Tegel, and D. Johrendt, Phys. Rev. Lett. **101**, 107006 (2008).
[5] J. Dong, H. J. Zhang, G. Xu, Z. Li, G. Li, W. Z. Hu, D. Wu, G. F. Chen, X. Dai, J. L. Luo, Z. Fang, and N. L. Wang, EPL **83**, 27006 (2008).
[6] S. Sharma, S. Shallcross, J. K. Dewhurst, A. Sanna, C. Bersier, S. Massidda, and E. K. U. Gross, Phys. Rev. B **80**, 184502 (2009).
[7] D. J. Singh and M.-H. Du, Phys. Rev. Lett. **100**, 237003 (2008).
[8] I. I. Mazin, D. J. Singh, M. D. Johannes, and M. H. Du, Phys. Rev. Lett. **101**, 057003 (2008).
[9] G. Xu, W. Ming, Y. Yao, X. Dai, S. C. Zhang, and Z. Fang, EPL **82**, 67002 (2008).
[10] C. Cao, P. J. Hirschfeld, and H.-P. Cheng, Phys. Rev. B **77**, 220506(R) (2008).
[11] A. N. Yaresko, G.-Q. Liu, V. N. Antonov, and O. K. Andersen, Phys. Rev. B **79**, 144421 (2009).

[12] K. Haule, J. H. Shim, and G. Kotliar, Phys. Rev. Lett. **100**, 226402 (2008).
[13] M. R. Norman, Phys. **1**, 21 (2008), and referencies therein.
[14] S. Wakimoto, K. Kodama, M. Ishikado, M. Matsuda, R. Kajimoto, M. Arai, K. Kakurai, F. Esaka, A. Iyo, H. Kito, H. Eisaki, and S. Shamoto, arXiv:0906.2453 (unpublished).
[15] V. I. Anisimov, Dm. M. Korotin, M. A. Korotin, A. V. Kozhevnikov, J. Kunes, A. O. Shorikov, S. L. Skornyakov, and S. V. Streltsov, J. Phys.: Condens. Matter **21**, 075602 (2009).
[16] L. Boeri, O. V. Dolgov, and A. A. Golubov, Phys. Rev. Lett. **101**, 026403 (2008).
[17] T. Yildirim, Physica C **469**, 425 (2009).
[18] F. Yndurain and J. M. Soler, Phys. Rev. B **79**, 134506 (2009).
[19] C. Liu, T. Kondo, M. Tillman, R. Gordon, G. Samolyuk, Y. Lee, C. Martin, J. L. McChesney, S. Bud'ko, M. Tanatar, E. Rotenberg, P. Canfield, R. Prozorov, B. Harmon, and A. Kaminski, arXiv:0806.2147 (unpublished).
[20] N. F. Berk and J. R. Schrieffer, Phys. Rev. Lett. **17**, 433 (1966).
[21] S. Raghu, X. L. Qi, C. X. Liu, D. J. Scalapino and S. C. Zhang, Phys. Rev. B **77**, 220503(R) (2008).
[22] K. Kuroki, H. Usui, S. Onari, R. Arita, and H. Aoki, Phys. Rev. B **79**, 224511 (2009).
[23] A. V. Chubukov, D. V. Efremov, and I. Eremin, Phys. Rev. B **78**, 134512 (2008).
[24] U. von Barth and L. Hedin, J. Phys. C **5**, 1629 (1972).
[25] I. I. Mazin, M. D. Johannes, L. Boeri, K. Koepernik, and D. J. Singh, Phys. Rev. B **78**, 085104 (2008).
[26] Z. P. Yin, S. Lebegue, M. J. Han, B. P. Neal, S. Y. Savrasov, and W. E. Pickett, Phys. Rev. Lett. **101**, 047001 (2008).
[27] Q. Huang, J. Zhao, J. W. Lynn, G. F. Chen, J. L. Luo, N. L. Wang, and P. Dai, Phys. Rev. B **78**, 054529 (2008).
[28] We have compared the band structures obtained using the rigid-band model and virtual crystal approximation (VCA). Within an energy window of 3 eV around the Fermi energy the electronic bands are identical (with maximum deviation up to 40 meV). Beyond this energy range deviations up to 200 meV were observed. These differences should not visibly effect the results. Larger differences between rigid-band model and VCA were observed by P. Larson and S. Satpathy, Phys. Rev. B **79**, 054502 (2009). Obviously, a calculation of χ_0 within a supercell approach is computationally intractable.
[29] G. F. Giuliani and G. Vignale, *Quantum Theory of the Electron Liquid* (Cambridge University Press, Cambridge, England, 2005).